Structural, Physical, Electrical and Dielectric Properties of Magnetic Glasses: $x\mathrm{Fe_2O_3} + (30 - x)\mathrm{V_2O_5} + 30\mathrm{Na_2O} + 40\mathrm{B_2O_3}$ with $x = 0$ to 15

P. Chand[a,b,*], L. Kumar[b], A. Yadav[c] and S. Khasa[d]

[a]Department of Physics, Netaji Subhas University of Technology, Sector 3, Dwarka, New Delhi — 110078, India

[b]Material Science, Department of Physics, SRM University, Delhi-NCR Sonepat — 131029, Haryana, India

[c]Department of Applied Physics, Delhi Technological University, Delhi — 110042, India

[d]Materials Research Laboratory, Department of Physics, DCR University of Science and Technology, Sonepat — 131039, Haryana, India

(Received April 14, 2019; revised version October 1, 2019, in final form November 4, 2019)

Magnetic glasses compositions: $x\mathrm{Fe_2O_3} + (30 - x)\mathrm{V_2O_5} + 30\mathrm{Na_2O} + 40\mathrm{B_2O_3}$ (x = 0, 2, 3, 5, 7, 10, and 15), abbreviated as FVNBx, are prepared with conventional melt-quenching technique, and the structural, physical, and electrical properties of compositions are investigated. The amorphous nature of the FVNBx glasses is confirmed using X-ray diffraction technique. It is found that the density of the glasses increases with x. The molar volumes calculations are based on the molar mass and the density data, which are then correlated with the structural changes. The decrease in the theoretical optical basicity shows marginal increase in the covalence of oxygen, when the V_2O_5 content is replaced with Fe_2O_3. The Fourier transform infrared spectroscopy that is carried out in the mid-IR region, shows the absence of the six-atomic (B_3O_3) boroxol rings. In this paper, the IR absorption bands corresponding to the combined contributions of tri and tetra borate vibrations are identified. The distinct IR spectra of the samples with different x indicates that the iron acts as a strong glass modifier, and brings only noticeable microstructural changes in the glass structures. Fe_2O_3 is believed to act as both glass former and glass modifier. The increase of DC electrical conductivity with temperature indicates a semiconducting nature of the glasses. The replacement of V_2O_5 by Fe_2O_3, even by 1 mol%, decreases the DC conductivity by an order of magnitude, and increases the activation energy by a factor of two. Composition, frequency, and temperature dependence of different dielectric parameters, namely dielectric constant ε', dielectric loss ε'', loss tangent $\tan(\delta)$, electrical modulus M^*, etc., are also analyzed.

DOI: 10.12693/APhysPolA.136.897

PACS/topics: soda-iron-boro-vanadate glasses, FTIR, dielectric, electrical conductivity, electrical modulus, loss tangent

1. Introduction

Glasses form a very distinct class of materials, which become important due to its countless applications. Traditional use of glasses includes containers, windows, lamps and optical components etc. More specific use includes applications in communication, electronics, and containers for radioactive waste. Any development that demonstrates the importance, versatility, and promise of glasses for newer and newer use, makes these materials very attractive for researchers. The glasses are prepared by almost limitless different chemical compositions, which give rise to different properties. Borate glasses are known for lower temperature fabrication, variety of chemical compositions, and for their structural peculiarities. This is due to their dielectric, optical, magnetic, and super ionic properties [1–5].

The structural information is usually obtained by X-ray and infrared investigations. The thermal study provides information about the stability and the glass transition temperature. The electrical properties are investigated by the dielectric measurements and the AC and DC electric conductivities.

From previous studies on glasses, it is well understood that glasses can exhibit both electronic conduction as well as polaronic one. This latter conduction is directly dependent on the local structure and carrier concentration in the material under study. Jozwiak et al. had investigated the electrical and thermal properties of lithium–iron–phosphate (LFP) glasses and found that glasses with olivine-like local order exhibit mixed polaronic–ionic conductivity with predominance of the polaronic component [6]. They have also shown the possibility of enhancement in total electrical conductivity by the creation of nanocrystallites in the lithium–iron–phosphate glass. Garbarczyk et al. [7] have studied electrical properties of mixed conductive silver vanadate–phosphate glasses and observed the ion-polaron effect (IPE) due to electrostatic attraction

*corresponding author; e-mail: prem@iitk.ac.in

between electrons/polarons and Ag^+ ions. This IPE effect results in decrease of total electrical conductivity at specifically given concentrations of both components. Kamitsos et al. have studied the lithium sulfate based fast ionic conducting borate glasses by vibrational and electric transport measurements. They found an evidence for two broad distributions of cation-hosting environments [8, 9]. Bih et al. studied the electronic and ionic conductivity of glasses of the Li_2O–MoO_3–P_2O_5 system [10]. Recently, Langar et al. investigated the conductivity and dielectric behaviour of $NaPO_3$–ZnO–V_2O_5 glasses [11]. Mekki et al. have investigated the structure and magnetic properties of vanadium–sodium–silicate glasses [12]. Bhagat studied the dielectric relaxation in Na-doped BiPbSrCaCuO glasses [13]. Dalba et al. have investigated the short range order in borate glasses by X-ray absorption spectroscopy [14]. An electrothermal model for high field conduction and switching phenomena in Te_2O_2–V_2O_5 glasses was suggested by Montani et al. [15].

Our recent studies concern various properties of different vanadium doped borate glasses [16–18]. Kashif et al. have studied the effect of alkali content on AC conductivity of borate glasses containing two transition metals [19]. Borate glasses are generally insulating in nature and the addition of transition metal oxides, such as Fe_2O_3 and V_2O_5, makes them dilute magnetic in nature and electrically semiconducting. These mentioned properties create possibilities for preparing such glasses having potential applications in optical and electronic memory switching, cathode materials for making solid state devices, and optical fibres. Addition of alkali metal oxides to borate network results in the formation of several borate groups, which lead to tightly organized structures in an intermediate range order. Alkali borate glasses having transition metal ions could open up new possibilities to extend the properties of these materials.

Mekki et al. reported that in vanadium–sodium–silicate glasses only 2% of total vanadium was found in magnetic V^{4+} oxidation state, most of it was found to exist in the non-magnetic V^{5+} oxidation state [12]. Saetova et al. have studied the Li_2O–V_2O_5–B_2O_3 glasses and, similarly to borate case, found that vanadium exists predominantly in non-magnetic V^{5+} valence whereas the magnetic V^{4+} valence is in minority, while the electrical conduction is mainly electronic [20].

There exists such a conviction that the increase in the average spacing between the polaron hoping sites inhibits the mobility of small polarons. Thus, observed decrease in the electrical conductivity and increase in the activation energy might be affected by increase in energy hopping. Network modification reveals the formation of non-bridging oxygens (NBOs), and converting basic structural units of borate and vanadate into charged units. The concentration of the NBOs determines ease of bond reconstruction and hence the viscosity. The microstructural information is conventionally obtained through characteristic Fourier transform infrared (FTIR) spectra, X-ray diffraction (XRD), and other spectroscopic techniques. Presence of iron in the glasses ensures that these glasses are magnetic since both Fe^{2+} and Fe^{3+} oxidation states are magnetic, whereas vanadium can exist entirely in non-magnetic V^{5+} oxidation state.

In the present paper, we have attempted to study the magnetic soda–boro–vanadate–iron glasses of the composition: $x\mathrm{Fe_2O_3} + (30 - x)\mathrm{V_2O_5}{+}30\mathrm{Na_2O} + 40\mathrm{B_2O_3}$ (FVNBx, where $x = 0, 2, \ldots, 15$). Results of physical, structural, thermal, and electrical measurements on the FVNBx glasses are presented.

2. Experimental

2.1. Glass preparation

The glasses of the desired composition were prepared by the conventional quick melt quenching technique. The starting materials were analytical grade reagents (AnalaR): H_3BO_3, Na_2CO_3, V_2O_5 and Fe_2O_3. The desired amounts of components were calculated according to the molar formula $x\mathrm{Fe_2O_3} + (30 - x)\mathrm{V_2O_5} + 30\mathrm{Na_2O} + 40\mathrm{B_2O_3}$ (abbreviated as FVNBx), where x = 0, 2, 3, 5, 7, 10, and 15 mol%. Appropriate amounts of Fe_2O_3, V_2O_5, Na_2CO_3, H_3BO_3 were well dry mixed and homogenized. The homogenized powders were melted in high purity alumina crucibles maintained at a temperature of 1050 °C in an electrically heated muffle furnace for about one hour. The alumina crucibles containing glass melts were swirled frequently to insure the homogeneity of the melt. The melts were then quickly quenched to lower temperature ($\approx$ 300 °C) by pouring onto clean thick stainless steel (SS) plates preheated to $\approx$ 300 °C and subsequently pressing by another thick SS plate which was preheated to $\approx$ 300 °C to provide a better quenching rate, to reduce the strains during glass formation, and to obtain smooth surfaces of the plate-glass samples.

2.2. XRD

The as prepared samples were crushed to a fine powder and analysed using X-ray diffractometer (RigakuUltima IV) by employing Cu K_α radiations. The diffraction patterns were taken for two-theta (2Θ) from 20° to 80° at a scan speed of 2° per min.

2.3. Density measurement

The density D of the prepared glass samples was measured using the Archimedes principle at room temperature RT. The masses of the samples were measured by sensitive electronic balance (CAS CAVY 220). Xylene was used as an inert immersion liquid for measuring the buoyancy. The density was calculated using the formula

$$D = \frac{D_\chi W_a}{W_a - W_\chi}, \tag{1}$$

where D_χ, W_a, and W_χ are the xylene density, the weight of sample in air, and the weight of sample in buoyant liquid (here xylene), respectively. The molar volume V_m of each glass sample was calculated from data obtained for density. Overall, the formula $V_m = M/D$ was used, where M is molar mass of samples. The error in the density measurement was estimated as ± 0.01 g/cc (1 g/cc $= 10^3$ kg/m^3).

The theoretical optical basicity (Λ_{th}) was calculated by using the following relation:

$$\Lambda_{th} = X_{Fe_2O_3}\Lambda_{Fe_2O_3} + X_{V_2O_5}\Lambda_{V_2O_5} + X_{Na_2O}\Lambda_{Na_2O} + X_{B_2O_3}\Lambda_{B_2O_3}. \quad (2)$$

Here, X-terms are mole fractions and Λ-terms are optical basicity values of corresponding oxides, as assigned in literature [21–24].

2.4. Thermal analysis — differential scanning calorimetry

The differential scanning calorimetry (DSC) measurements of the samples in the bulk form were carried out in the temperature range of RT to 900 °C on a simultaneous thermal analyzer (Perkin Elmer STA 6000). The heating rate and nitrogen flow rate used to carry out the analysis were 10 °C/min and 100 ml/min, respectively. The differential temperature versus temperature (ΔT vs. T) and loss of mass versus temperature (Δm vs. T) were recorded and plotted. ΔT is taken as positive for the endothermic process. For loss of mass at different temperatures the mass of the sample under test is monitored as a function of temperature under the flow of hot dry nitrogen gas and then loss of mass in percent (Δm) is calculated as a function of temperature T.

2.5. FTIR

The FTIR spectra of the glass samples were recorded at room temperature on Perkin Elmer Frontier FTIR spectrometer in the mid-IR range, i.e., 400–4000 cm^{-1}. To record the infrared absorption spectra, KBr pellet technique was used. Base line and noise correction were achieved using Spectrum-10 software (provided with FTIR spectrophotometer). For peak identification of the processed spectra, multiple peaks fitting of each spectrum was carried out using *Origin-16 Pro* by adding peaks till the fit parameter became ≥ 0.999.

2.6. Electrical measurements

For these measurements, samples were cut and polished in the form of rectangular plates with the thickness ranging $\approx$ 1.0 mm. The broad faces of the regular shaped glass sample were painted by colloidal silver paste to remove any type of surface irregularity and to form two conducting electrodes. Since the samples showed high resistivity, the DC electrical conductivity of samples was measured by two probe method in the temperature range from RT to 200 °C with a heating rate of 1 °C/min. All the measurements were carried out on a Keithley low voltage source meter (Model 2401) in 4 wire mode and by applying a filter with repeated average of 50 points. A constant voltage of 20 V was applied across the high and low terminals while carrying out measurements. To avoid degradation of the samples, current was passed only for short periods (less than 20 s at a time). To avoid any sort of polarization effect, a toggle switch was used to reverse the polarity of applied voltage frequently at each measurement and the value of current was taken as an average of the maximal DC electric current values for both forward and reverse polarities. For a body with a constant cross-section A (m^2) and a constant thickness t (m) carrying a current I (ampere) under the applied DC voltage V (V), the volume conductivity σ (S/m) of the specimen can be determined from the elementary formula: $\sigma = [(tI)/(VA)]$. The estimated error in the measurement of σ is about 3%.

The measurements at frequency lower than 1 kHz has not been reported because of instrument limitations as it gives fully noisy and insignificant data for those frequencies. Impedance spectroscopy of samples was carried out on an impedance analyzer *(Hioki 3532-50 LCR HiTester)* in a frequency range of 1 kHz to 5 MHz and temperature range from RT to 200 °C with a heating rate of 1 °C/min controlled through a digital programmable electrical furnace. The experimental errors in the capacitance and resistance measurements were estimated to be ± 0.1 pF and ± 10 Ω, respectively. The complex dielectric permittivity, $\varepsilon^* = \varepsilon' - j\,\varepsilon''$ (with ε' and ε'' as the real and the imaginary part of dielectric constant), dielectric loss tangent $\tan(\delta)$ and AC conductivity σ_{ac} were calculated from the standard relations

$$\varepsilon' = Ct/\varepsilon_0 A, \quad (3a)$$

$$\varepsilon'' = \varepsilon' \tan(\delta), \quad (3b)$$

$$\sigma_{ac} = 2\pi f \varepsilon' \varepsilon_0 \tan(\delta), \quad (3c)$$

where the symbols used are capacitance C (in F), area of broad cross-section A (in m^2), thickness t (in m), permittivity of free space $\varepsilon_0 = 8.854$ pF/m, and f (in Hz) is the frequency of AC voltage used in the experiment.

3. Results and discussion

3.1. XRD

The glass samples were tested by XRD to confirm the glassy nature of all the samples. The XRD patterns are shown in Fig. 1. All the samples have shown only characteristic glass XRD patterns. No crystalline phase is detected by XRD. This confirms the non-crystalline nature of the samples prepared for study.

3.2. Density

Measured values of density and calculated values of molar volume are collated in Table I. There is a distinct variation in the densities of the glasses depending on the iron and vanadium contents. Figure 2 displays the variation of the density as a function of iron content x.

TABLE I

Composition, density D, molar volume V_m, theoretical optical basicity Λ_{th} of FVNBx ($x = 0, 2, 3, 5, 7, 10, 15$) glasses.

x	Sample	Molar weight [g]	Density [g/cm^3]	Molar volume [cm^3/mol]	Optical basicity
0	0 Fe_2O_3 + 30 V_2O_5 + 30 Na_2O + 40 B_2O_3	136.78	2.42	56.43	0.902
2	2 Fe_2O_3 +28 V_2O_5 + 30 Na_2O + 40 B_2O_3	136.47	2.53	53.87	0.9016
3	3 Fe_2O_3 + 27 V_2O_5 + 30 Na_2O + 40 B_2O_3	136.32	2.57	53.12	0.9014
5	5 Fe_2O_3 +25 V_2O_5 + 30 Na_2O + 40 B_2O_3	136.00	2.59	52.41	0.901
7	7 Fe_2O_3 + 23 V_2O_5 + 30 Na_2O+ 40 B_2O_3	135.69	2.63	51.55	0.9006
10	10 Fe_2O_3 + 20 V_2O_5 + 30 Na_2O+ 40 B_2O_3	135.22	2.67	50.59	0.9000
15	15 Fe_2O_3 + 15 V_2O_5 + 30 Na_2O + 40 B_2O_3	134.44	2.72	49.46	0.899

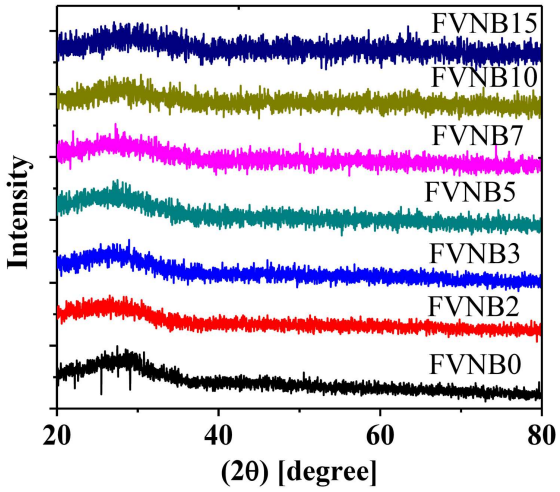

Fig. 1. XRD spectra of FVNBx ($x = 0$, 2, 3, 5, 7, 10, 15) glasses recorded at RT.

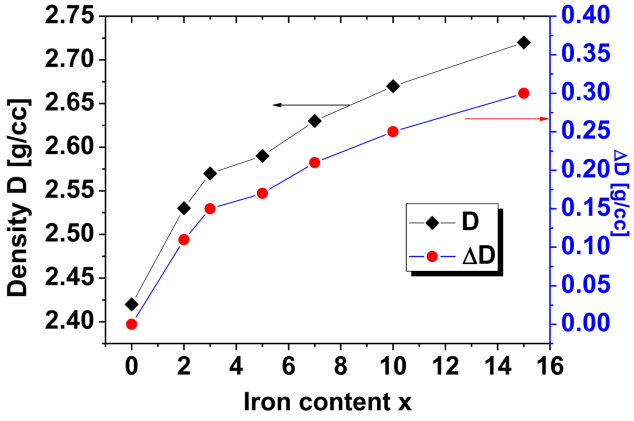

Fig. 2. Density variation of FVNBx ($x = 0$, 2, 3, 5, 7, 10, 15) glasses. ΔD represents the change in density with respect to FVNB0.

As can be seen, the overall change in density is around 0.3 g/cc when replacing V_2O_5 with increasing concentration of Fe_2O_3 (from $x = 0$ to $x = 15$). The increase in density and decrease in molar volume with the increase in iron content is justified because glass modifier V is being replaced by heavier metal iron and a better filling factor is created by Fe–O coordination in the glass microstructure by acting both as glass former and glass modifier.

The optical basicity proposed by Duffy and Ingram was used as a measure of acid-base properties of oxide glasses and is expressed in terms of the electron density carried by oxygen [25–28]. The values of theoretical optical basicity for the prepared compositions (as shown in Table I) indicate a nominal decrease with an increase in Fe_2O_3 content at the cost of V_2O_5 in the glass. The decreasing optical basicity by addition of Fe_2O_3 in place of V_2O_5 indicates a marginal decrease in the ability of oxygen to donate negative charge to the bonding. It points towards an increase in covalent character of the bonds in the glass network with increase in Fe_2O_3 content. This property may affect the electrical conduction of the glasses and a decrease in conductivity is anticipated.

3.3. Thermal analysis

From the ΔT versus T scans the glass transition T_g could be estimated from the broad endothermic shift as shown in Fig. 3 for all FVNBx ($x = 0$, 2, 3, 5, 7, 10, 15) glasses. The glass transition temperature T_g is considered to be a characteristic of structural relaxations taking place in the glass network and depends upon many factors, namely, bond strength, cross linking density, enthalpy of atomization, nature of the structural units constituting the glass network and their connectivity way [29, 30]. It was observed that the glass transition lies approximately between 500 °C and 550 °C (±25 °C) for all the glasses prepared. Further, by close analysis of Fig. 3, an increase in T_g is indicative with the increase of iron content x. This may be due to the reason that with increase in iron content, the inter atomic distance decreases and overall structure become more closely packed, i.e., density and bond strength increased and more energy is required to dissociate Fe–O and V–O bonds. This will cause an increase in transition temperature T_g with increase in iron content [31, 32]. This indicates that the Fe_2O_3 acts both as glass former and as glass modifier. To determine the thermal stability of the prepared glasses a known amount of the sample was heated with dry

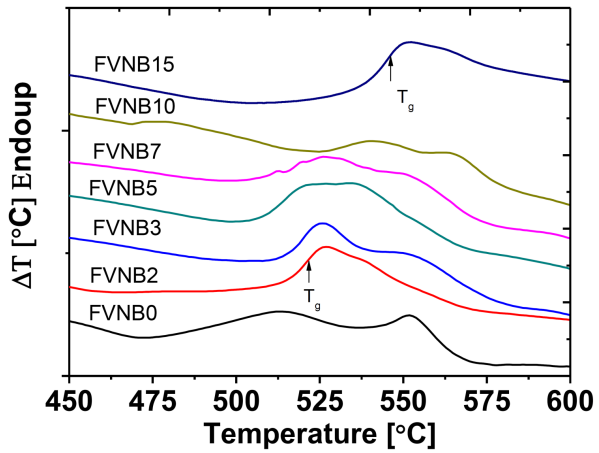

Fig. 3. Differential temperature ΔT vs. temperature T scans of FVNBx (x = 0, 2, 3, 5, 7, 10, 15) glasses. ΔT upward indicates the endothermic process.

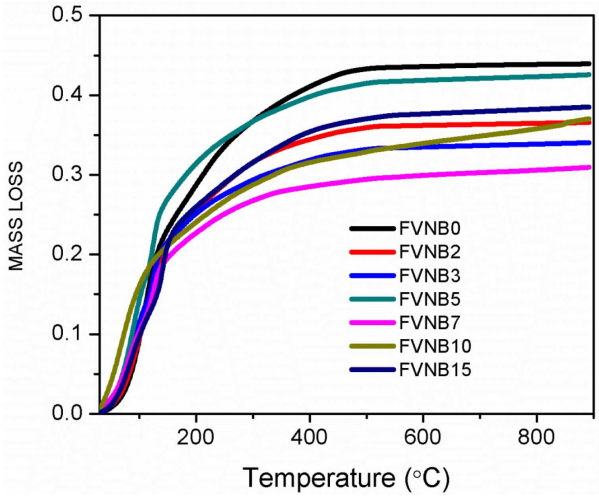

Fig. 4. Percent mass loss vs. T scans of FVNBx (x = 0, 2, 3, 5, 7, 10, 15).

nitrogen gas flow at a constant rate and the corresponding mass loss percent $\Delta m = 100(m_T - m_{RT})/m_{RT}$ was measured at different temperatures. Here, m_{RT} and m_T are the masses of the sample at RT and at temperature T, respectively. The measurements were performed on powdered samples. As prepared glass wafers were crushed to fine powders in a mortar and pestle under ambient conditions which were subsequently used for the mass loss measurements. The observed mass losses (in %) vs. temperature are shown in Fig. 4.

The observed percent mass losses lie in the range from 0.25 to 0.45 in the glass samples under investigation in the temperature range of study. The small mass loss is attributed to the evolution of the adsorbed moisture and ambient gases during the handling of the glass powders. It may also be mentioned that at RT no detectable mass loss was observed even after one year of the vacuum dry storage. This confirms that the prepared glasses are chemically stable over the temperature range of study.

3.4. FTIR study

The FTIR spectra of FVNBx glass systems at RT in the frequency range of 400–1600 cm^{-1} are shown in Fig. 5.

According to an assumption in vibrational spectroscopy of the solid state, the vibrations of a specific group of atoms in a lattice are regarded as relatively independent of motions of the rest of the atoms. In FTIR specific groups of atoms are characterized by distinct normal modes of vibrations and are displayed as absorption bands. The FTIR spectra show multiple absorption peaks which are attributed to different vibrational modes of various multi-atomic species existing the glass matrix (see Table II).

To analyze the FTIR spectra more accurately, multiple peak fittings of the FTIR spectra have been done using Origin 8.1Pro. Peaks were fitted to the simulated curve till the fit parameter became > 0.999. Gaussian peak fitted/convoluted spectra for all the samples are shown in Fig. 6. Through the peak fitting, the peak position/centre (cm^{-1}) and the relative area (intensity) of the peaks were determined. The data thus obtained is collated in Table III.

The FTIR spectra of sodium–iron–boro–vanadate glasses are expected to mainly consist of three absorption regions: (i) high frequency range 1200–1600 cm^{-1} attributed to the vibrations of B–O in borate units, in which boron is connected to three oxygen atoms (both bridging (BO) and non-bridging (NBO) types), (ii) mid frequency range 800–1200 cm^{-1}, which are mainly formed by tetrahedral coordinated boron (BO_4), and (iii) low frequency ranges 400–800 cm^{-1}, which are due to B–O–B and V–O–V bending and stretching of Fe–O (tetrahedral FeO_4 and octahedral FeO_6 units).

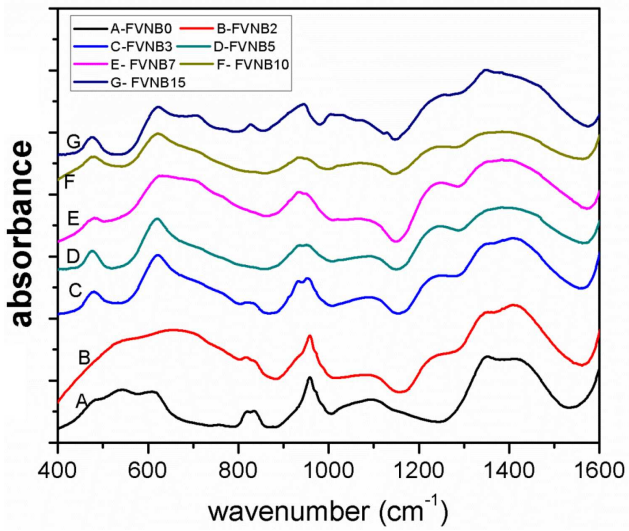

Fig. 5. FTIR spectra of FVNBx (x = 0, 2, 3, 5, 7, 10, 15) glasses recorded at RT.

TABLE II

Expected assignment of IR bands in the spectra of FVNBx [25, 26].

Peak position [cm^{-1}]	Assignment
∼ 1200–1400	stretching of B–O of trigonal boron (BO_3)
∼ 1250	stretching of trigonal boron connected to V atoms in borovanadate species $(B_2V_2O_9)^{2-}$
∼ 900–1100	stretching B–O of tetrahedral boron (BO_4)
∼ 950–1000 (sharp)	V=O stretching of vanadyl $(VO)^{2+}$
∼ 900–1050	stretching of four connected five-coordinated vanadium species (V^{4-}) $(VOO_4)^{2-}$
∼ 790–800	Stretching of two connected four coordinated vanadium species (V_2^-) $(VOO_2O)^-$
∼ 700–710	vibrations involving VOO_3^-
∼ 660	stretching modes of Fe–O of tetrahedral FeO_4
∼ 610–700	B–O–B bending of trigonal boron atoms
∼ 460–530	stretching modes of Fe–O of octahedral FeO_6
∼ 430–450	V–O–V bending modes

The absence of the prominent peak ≈ 800 cm^{-1} in the IR spectra of the present glasses is an indication of the missing six-member boroxol rings –(B_3O_3)– in the glass network. Based on the relative intensity the observed absorption bands are categorized as weak (W), medium (M) or strong (S) (see Table III).

In the present glasses, the main IR absorption peaks are present around: {614(M), 650–702(S), 921FVNB15, 944–960, 1050–1096, 1200–1275, 1330–1400, 1445, 1474, 1540, 1592} cm^{-1}. Asymmetric vibrations of B–O bonds from pyro- and ortho-borate groups in BO_3 trigonal units are confirmed from the peaks in the range 1200–1500 cm^{-1}. The IR spectrum of vitreous V_2O_5 is found similar to that of the crystal. It shows a sharp band around 950–1000 cm^{-1}, which means that the isolated V=O bonds from the VO_5 trigonal bipyramids are preserved also in the vitreous structure. The strong bands around 650–702 cm^{-1} are attributed to the bending vibrations of the O–V–O bond. The bands around 650–702 cm^{-1} are assigned to the combination vibrations of $(VO_3)_n$ single chain or due to antisymmetric vibrational modes of V–O–V group. The bands around 929–1007 cm^{-1} are attributed to the symmetric stretching vibrations of V–O–V. The main coordination polyhedron for vanadium in the crystal structures is the VO_4 tetrahedron with three terminal V–O bonds forming VO_3 groups. In the vitreous V_2O_5 counterpart, there is a band at ≈ 920 cm^{-1}, which is close to the symmetrical stretching vibrations of VO_3 unit, in the spectra of crystals. This band is observed in the FTIR spectrum of FVNB15 glass. The bands around 950–970 cm^{-1} are attributed

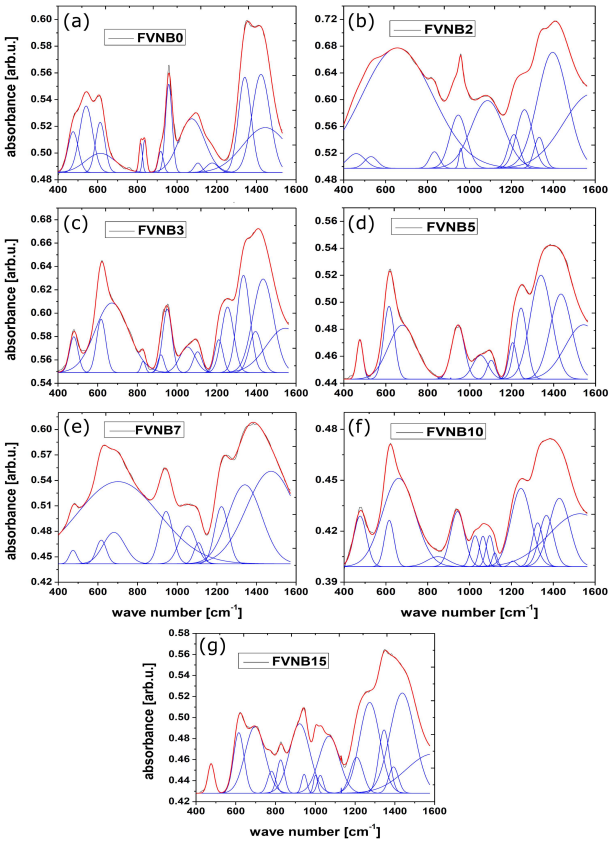

Fig. 6. Gaussian deconvoluted FTIR spectra for (a) FVNB0, (b) FVNB2, (c) FVNB3, (d) FVNB5, (e) FVNB7, (f) FVNB10, (g) FVNB15 glasses.

not only to the VO_5 groups but also to the branched VO_4 groups having one $(V=O)^{2+}$ double bond. This band has a medium to weak intensity in the present glasses. The weak presence of ν (V=O) band indicates that majority of the V exists in V^{5+} and V^{4+} valence is in minority. Such observation was confirmed by Saetova et al. in Li_2O–V_2O_5–B_2O_3 glasses. The absorption band at 1074 cm^{-1} in iron free FVNB0 glass shifts to a higher frequency (1086 cm^{-1}) in FVNB2 due to incorporation of two mole percent of Fe_2O_3. A shift to a higher frequency is attributed to shortening of B–O bond in di- and penta-borate linkages. However, this band remains stable 1152 cm^{-1} in FVNB3, FVNB5, and FVNB7 which indicates that a weakening of B–O bond has taken place for these concentrations of Fe_2O_3. For higher concentration of Fe_2O_3 ($x = 10$ and $x = 15$) a gradual shift towards higher frequency is observed which indicates a trend of strengthening of B–O bond for glasses containing higher iron content. The strong high frequency bands between 1300–1600 cm^{-1} attributed to O–B–O bonds of tetrahedral BO_4 and trigonal BO_3 bonds also show significant changes due to change in Fe_2O_3/V_2O_5 composition. The irregular trends in shifts of the frequencies confirm the changes in the structure of the glass network mainly through strengthening and/or weakening of the oxygen bonds (bridging and/or non-bridging).

TABLE III

FTIR peak centre [cm^{-1}] and relative peak area (intensity) for FVNBx glasses. The relative intensity is shown in parenthesis along with the peak centre [cm^{-1}]. Peaks with intensity (1)–(4) are termed as weak, with (5)–(9) as medium and above (9) as strong.

FVNB0	FVNB2	FVNB3	FVNB5	FVNB7	FVNB10	FVNB15
476(4)	460(1)	479(3)	476(2)	475(1)	477(5)	476(1)
542(9)	530(1)	–	–	–	–	–
613(5)	–	–	–	–	–	–
614(6)	–	617(5)	615(3)	617(1)	616(3)	615(5)
–	656(39)	671(20)	679(13)	681(4)	661(22)	697(10)
–	–	–	–	702(39)	–	–
817(1)	–	–	–	–	–	780(1)
837(1)	833(1)	829(1)	–	–	848(2)	826(2)
918(1)	–	919(1)	910(1)	–	–	921(10)
–	947(4)	–	944(6)	944(4)	942(6)	944(1)
958(1)	959(1)	951(5)	–	–	–	–
–	–	–	–	–	–	1001(1)
–	–	1020(1)	–	–	1026(2)	1025(1)
–	–	1052(3)	1051(3)	1053(4)	1064(2)	1069(9)
1074(14)	1086(9)	–	–	–	1096(2)	–
1105(1)	–	1104(2)	1102(1)	1107(1)	1120(1)	1130(1)
1177(1)	–	–	–	–	–	–
–	1212(2)	1210(2)	1205(3)	1224(4)	1207(1)	1208(3)
–	1263(4)	1255(3)	1245(4)	–	1245(11)	1274(14)
1342(12)	1333(1)	1335(11)	1340(20)	1341(15)	1325(4)	1346(5)
–	1397(16)	1395(5)	–	–	1367(5)	1393(2)
1423(18)	–	–	–	–	1429(11)	–
–	–	1434(18)	1435(17)	–	–	1438(19)
1445(21)	–	–	–	1474(26)	–	–
–	1584(19)	1546(15)	1543(18)	–	1527(25)	1592(16)

Another interesting feature is displayed by the shifts in the low frequency bands. The negligible shift in bands assigned to V–O bonds indicates a stable nature of the V–O bonds in the glass network of the glasses under study. However, a band ≈ 655 cm^{-1} assigned to Fe–O bond of tetrahedral FeO_4 units reflects a regular increase in frequency with x (except for $x = 10$). This confirms that the shortening of Fe–O bond is occurring in the tetrahedral FeO_4 units of the glass network as the Fe_2O_3 content is increased. Therefore the analysis of the FTIR spectra of the samples revealed significant changes in the features of the absorption bands which are a confirmed signature of the micro-structural changes in the glass network due to change of Fe/V composition. Therefore in the present glass system Fe_2O_3 acts both as glass modifier as well as glass former.

3.5. Electrical measurements

The temperature dependence of DC electrical conductivity σ of as prepared glasses are presented in Fig. 7. This dependence of the DC conductivity obeys the well known Arrhenius formula [16, 27, 28], namely

$$\sigma = \sigma_0 \exp\left(-\frac{W}{k_B T}\right), \tag{4}$$

where W is the activation energy for conduction, σ_0 is a constant for given glass, k_B is the Boltzmann constant and T is the temperature in kelvin (K). The values of W and pre-exponential factor σ_0, were evaluated by the least squares fitting of the experimental data, using the relation

$$\log(\sigma) = \log(\sigma_0) - \frac{W}{2303 k_B}\frac{1000}{T}. \tag{5}$$

This linear relationship between conductivity and reciprocal of temperature indicates that the activation energy is independent of temperature in the range studied here. The fact that σ increases with increase in temperature establishes the semiconducting type of behaviour for electrical conductivity. The calculated values of σ (at 80 °C and 180 °C), σ_0 and W are displayed in Table IV. The x dependence of DC conductivity at 80 °C and 180 °C are shown in Fig. 8 for comparison. The activation energy W vs. x plot is shown in Fig. 9. At 80 °C the conductivity is found to decrease as x is increased. The activation energy however, shows a reverse correlation with x, which is consistent with small polaron hopping (SPH) model [27, 28, 33] and explains the semiconducting nature of the glasses under study. At 180 °C the conductivity of FVNB10 glass increases as compared

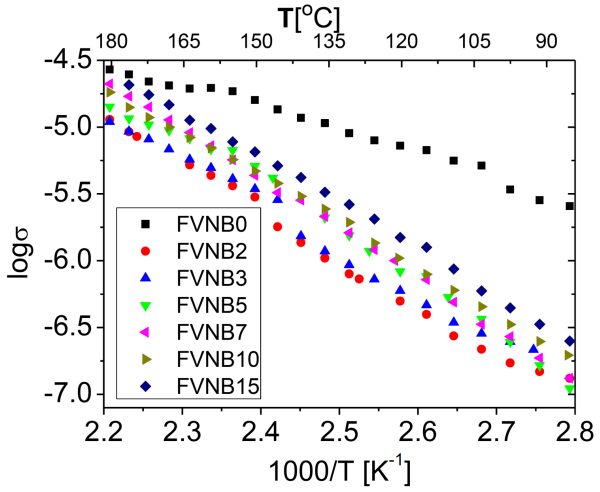

Fig. 7. Variation of $\log(\sigma_{dc})$ [S/m] as a function of reciprocal of temperature for FVNBx (x = 0, 2, 3, 5, 7, 10, 15) glasses.

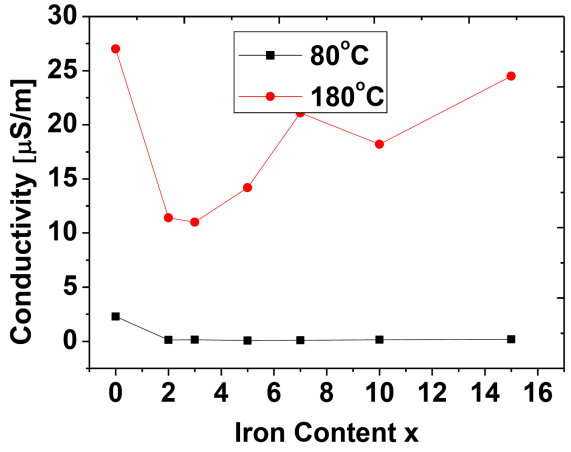

Fig. 8. DC conductivity at 80 °C and 180 °C for the FVNBx (x = 0, 2, 3, 5, 7, 10, 15) glasses.

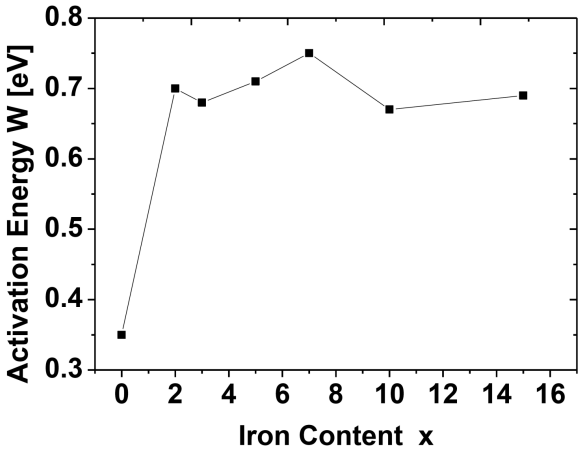

Fig. 9. Activation energy W of the FVNBx (x = 0, 2, 3, 5, 7, 10, 15) glasses.

TABLE IV

DC conductivity σ, prefactor σ_0 and activation energy W for FVNBx (x = 0, 2, 3, 5, 7, 10, 15) glasses

Sample	σ at 80 °C [μS/m]	σ at 180 °C [μS/m]	σ_0 [S/m]	W [eV]
FVNB0	2.3	27.0	0.21	0.35
FVNB2	0.12	11.4	744.6	0.70
FVNB3	0.14	11.0	397.2	0.68
FVNB5	0.07	14.2	1490.7	0.71
FVNB7	0.09	21.1	4243.3	0.75
FVNB10	0.01	18.2	564.9	0.67
FVNB15	0.02	24.5	1100.3	0.69

to FVNB7, but it decreases continually with further increase in x up to 15. The linear relationship between conductivity and reciprocal of temperature indicates that the activation energy is independent of temperature. As compared to the iron free glass FVNB0 the conductivity of iron containing $x > 0$ glasses decreases drastically (by an order of magnitude) with the inclusion of Fe_2O_3 in the glass network (the average value of σ at 80 °C being is 0.08 μS/m). The prominent conduction mechanism in V_2O_5 is due to electron hopping between V^{3+}, V^{4+}, and V^{5+} states and in mechanism in Fe_2O_3 is due to hopping in Fe^{2+}, Fe^{3+} ions. Recently, Pietrzak et al. [34] had studied the Li_2O–FeO–V_2O_5–P_2O_5 system by the Mössbauer spectroscopy and thermoelectric power measurements to find the most prominent hopping centre between iron or vanadium ions, which one is dominating the charge carrier transport in glass system. It has been found that Fe^{2+}/Fe^{3+} ratio does not have major influence on electronic conductivity possessed by dominating V^{4+}/V^{5+} hopping sites. Similar phenomenon is observed in conduction processes of presently prepared glass systems. With the increase in Fe_2O_3 content and consequent decrease in V_2O_5 content, the decrease in electrical conductivity implies that V^{4+}/V^{5+} ions in the present glass system create structural changes such that the charge carrier transport responsible for electrical conduction in the glass network is hindered. This may be translated to the increase in small polaron hopping (SPH) range/distance and resistance to polaron orientation motion (both jump as well as frequency). Within the iron containing glasses $x > 0$, the conductivity is minimal for FVNB10 glass at 80 °C and for FVNB3 at 180 °C, whereas it is maximal for FVNB3 at 180 °C and for FVNB15 at 180 °C. The total conductivity is due to carrier hopping in both types of ions, i.e., iron (less dominating) and vanadium (more dominating). Here, iron ions is replaced by more conducting vanadium ions, which results into the decreasing trend of electrical conductivity values [35].

Also the reduction in vanadium content may cause gradual reduction of conductivity if conduction due to electronic hopping $V^{4+} \Longleftrightarrow V^{5+}$ is envisaged due to expected increase in V–V distance with x. But the abrupt decrease in conduction upon replacing V by small amount

of Fe does not support this mechanism, too. Therefore, the conduction appears to be through the charge generated on the non bonding oxygens (NBOs) in the glass network through small range polaron hopping (SRPH) mechanism. The average activation energy for the iron containing glasses (i.e., $x > 0$) is 0.7 eV which may be assumed to be same for all the iron containing glasses FVNBx ($x = 2, \ldots, 15$) yet the conductivity of FVNB15 at 180 °C appears to be approaching the value of conductivity of iron free FVNB0 glass. This observation can be explained by the assumption that the small range polaron hopping (SRPH) frequency increases in the iron containing glasses as the temperature is raised. An increase in SRPH frequency at higher temperatures is justified due to available thermal excitation.

3.6. AC conductivity

Figure 10a shows the frequency dependence of AC conductivity σ_{ac} for FVNB0, FVNB5, and FVNB15 compositions at $T = 200$ °C and Fig. 10b shows the frequency dependence of σ_{ac} for FVNB5 at different temperatures. These are taken as representative cases since other samples also show similar trends. At lower frequency, conductivity is low and is almost independent of frequency. This is explained on the basis of space charge polarisation effect which is responsible for the large bulk resistance at lower frequencies. As a consequence, a plateau region is obtained (see Fig. 10), which shows the frequency independent part of conductivity or the absolute value of impedance. With further increase in frequency, dispersion at higher frequencies (in MHz range) has been observed at all the temperatures and in all the samples studied in this work. The dispersion at higher frequency shifts towards higher frequencies with an increase in temperature. Further, the conductivity spectrum has found [36] to obey the Jonscher power law (JPL) of the AC conductivity in glasses, which is mathematically written as

$$\sigma = \sigma_0 + A_1(f)^{s1} + A_2(f)^{s2}. \tag{6}$$

Here, σ_0 is the conductivity at limiting zero frequency (termed as frequency independent DC component of conductivity), A_1 and A_2 are constants, and s_1 and s_2 are the characteristic temperature dependent parameters. The power law exponents s_1 and s_2 (lies in the range

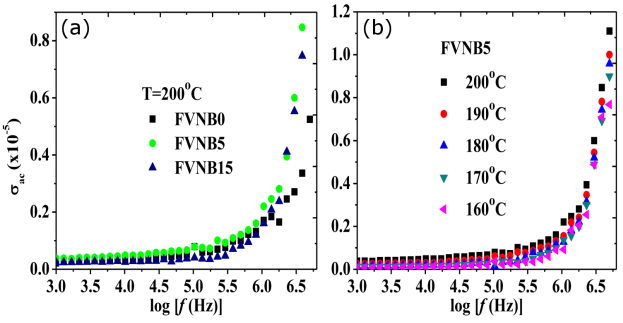

Fig. 10. Variation of σ_{ac} vs. $\log(f)$ [Hz] for (a) compositions FVNB0, FVNB5 and FVNB15 at temperature 200 °C, (b) FVNB5 at different temperatures.

TABLE V

Dielectric parameters and AC electrical conductivity of FVNBx glasses at 200 °C and at 5 MHz.

Sample	ε'	ε'' ($\times 10^{-2}$)	$\tan(\delta)$	M'	M''	σ_{ac} [μS/m] (at 5 MHz)
FVNB0	0.17	0.19	0.11	5.920	0.67	5.25
FVNB2	0.05	0.12	0.23	17.50	3.99	3.45
FVNB3	0.05	0.06	0.12	19.13	2.27	1.70
FVNB5	0.03	0.06	0.16	28.67	4.67	1.54
FVNB7	0.07	0.03	0.04	13.69	0.61	0.91
FVNB10	0.13	0.04	0.03	7.50	0.21	1.03
FVNB15	0.13	3.30	0.26	7.33	1.88	9.15

$0 < s_1, s_2 < 1$) represent the degree of interaction between the mobile ions [37]. The AC conductivity values at $T = 200$ °C and frequency 5 MHz for all prepared compositions are reported in Table V. The observed trend of change of σ_{ac} values is due to hindrance offered by mixed effect of iron and vanadium ions which further results into the polaronic conduction in prepared glasses [36]. It can be observed that σ_{ac} increases with increase in temperature, which is possibly due to depletion of space charge effect and thermally activated hopping of charge carriers [38–40]. It is quite interesting to note that the value of frequency independent conductivity measured at 1 kHz at 200 °C for iron containing $x > 0$ glasses is ≈ 0.07 μS/m, which is very near to the average DC conductivity (≈ 0.08 μS/m) calculated for prepared glasses at 80 °C (as shown in Fig. 8).

4. Dielectric properties

4.1. Dielectric loss

The variation of dielectric constant (ε') as a function of frequency at $T = 200$ °C is illustrated in Fig. 11a. For all the prepared compositions variation of ε' with frequency is not significant except in case of FVNB5 (shown in Fig. 11b). The frequency dependence of dielectric loss ε'' is shown in Fig. 12a, as a function of composition x, while in Fig. 12b the temperature dependence of ε'' for FVNB5 is shown. Various polarization mechanisms in dielectrics are: (i) electronic, (ii) ionic, (iii) dipole orientation/deformation in polar dielectrics, and (iv) migrational/space charge polarization [27]. The contribution of electronic polarization is negligible as compared to the other contributions due to ionic polarization and in non-polar dielectrics the main contribution comes from the last mechanism. The ionic polarization is frequency independent up to far IR frequencies. However, the orientation/deformation polarization and the migrational/space charge polarization are frequency dependent and usually decrease at higher frequencies. The ionic polarization is temperature independent but the orientational and the migrational polarizations are temperature dependent and while the former is expected to decrease due to thermal agitation the later is expected

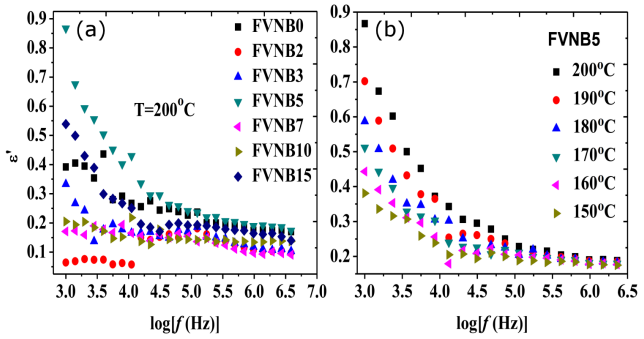

Fig. 11. Variation of ε' vs. $\log(f)$ [Hz]: (a) different compositions at 200 °C, (b) FVNB5 at different temperatures.

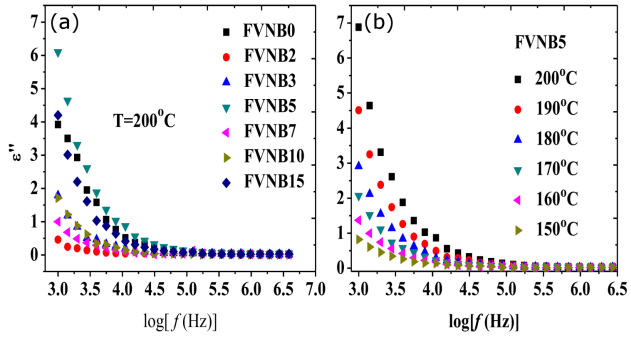

Fig. 12. Variation of ε'' vs. $\log(f)$ [Hz]: (a) different compositions at temperature 200 °C, (b) FVNB5 at different temperatures.

to increase with the rise in temperature. Study of literature [17, 18, 27, 28, 33, 38–40] suggests that in dielectric permittivity ε^* of a sample is due to (i) rotation of ions around their negative sites and (ii) short range dipole transport (hopping).

Analysis of ε' and ε'' shows that both the parameters have higher values at lower frequencies and the values become very small (frequency independent) at higher frequencies which is a signature of migration polarization in non-polar dielectrics. At lower frequencies, the space charge accumulation occurs at the electrolyte (glass)–electrode interface, which does not permit further transfer of the ions through the dielectric. At the higher frequencies, the periodic reversal of electric field occurs and the polarization due to accumulation of charge decreases and causes a decrease in the values of ε' and ε'' with the increase in frequency [37–41]. The variations of ε' and ε'' as a function of frequency for FVNB5 at different temperatures are shown in Fig. 11b and Fig. 12b, respectively. The effect of temperature change is significantly observed at lower frequencies on ε' and ε''. At lower frequencies, the value of ε' and ε'' increases with temperature whereas at higher frequencies, variation in ε' and ε'' has been found more or less independent of temperature and frequency. This occurs due to weakening of bonds

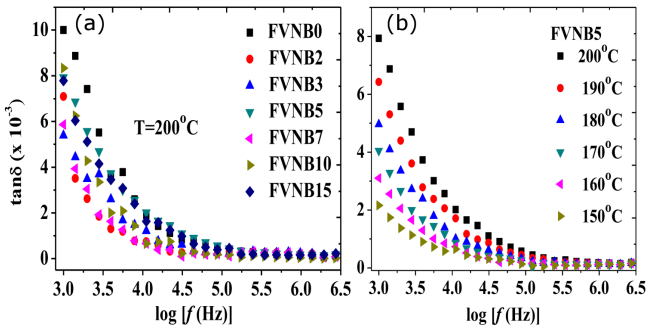

Fig. 13. Variation of $\tan(\delta)$ vs. $\log(f)$ [Hz]: (a) different compositions at 200 °C, (b) FVNB5 at different temperatures.

and an increase in thermal agitation that causes a disturbance in the orientational vibrations of the molecular groups in glass network. Therefore, space charge polarization decreases with increase in temperature [39].

4.2. Loss tangent ($\tan(\delta)$)

Figure 13a shows the frequency dependence of dielectric loss tangent ($\tan(\delta)$) for all the prepared FVNBx compositions. The variation of $\tan(\delta)$ with frequency at constant temperature exhibits similar trends as for ε'' which could be due to the fact that as the frequency increases, the polarizability contribution from ionic and orientation sources decreases and finally disappears due to their inertia. Figure 13b shows the frequency dependence of dielectric loss tangent for FVNB5 at different temperatures. The dielectric loss is seen to decrease for $x = 7$ and $x = 10$ as compared to other glasses. The variation of dielectric parameters upon changing the Fe/V content verifies the structural changes in the glass networks although no regular trend is visualized.

4.3. Modulus formalism

To analyze the relaxation data, we often need to represent the dielectric as a combination of pure resistances and capacitances and the manner of their connection is assumed. Relaxations in such circuits can proceed through two independent processes known as serial and parallel processes. Macedo et al. [40] proposed on the basis that impedances are additive in a series process and used electrical modulus, $M^* = 1/\varepsilon^*$, as appropriate parameter for the analysis of conductivity relaxation. Therefore, M^* is also resolved into real and imaginary parts as

$$M^* = \frac{1}{\varepsilon^*} = \frac{\varepsilon'}{(\varepsilon')^2 + (\varepsilon'')^2} + \frac{\varepsilon''}{(\varepsilon')^2 + (\varepsilon'')^2}. \tag{7}$$

Redefining Eq. (3) by using ε_s to represent frequency independent dielectric constant and introducing $\tau_\sigma = \varepsilon_0 \varepsilon_s / \sigma_0$ and $M_s = 1/\varepsilon_s$, we come to the relation $M^* = M' + M''$, written as

$$M^* = M_s \left(\frac{\mathrm{i}\omega\tau_\sigma}{1 + \mathrm{i}\omega\tau_\sigma} \right) = M_s \left(\frac{(\omega\tau_\sigma)^2 + \mathrm{i}\omega\tau_\sigma}{1 + (\omega\,\tau_\sigma)^2} \right). \tag{8}$$

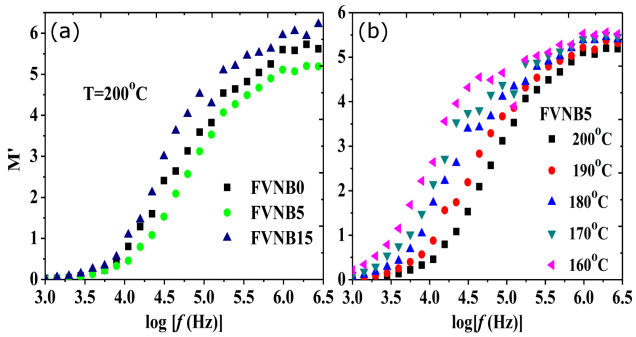

Fig. 14. Variation of M' vs. log(f) [Hz] for (a) compositions FVNB0, FVNB5 and FVNB15 at temperature 200 °C, (b) FVNB5 at different temperatures.

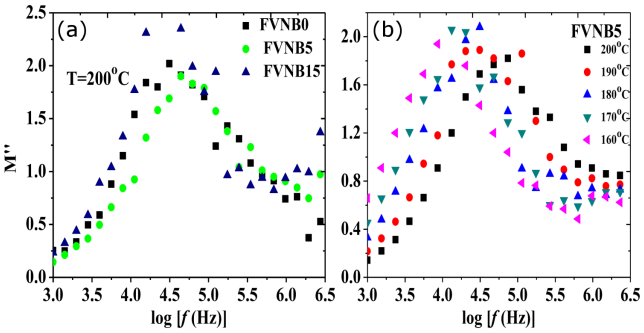

Fig. 15. Variation of M'' vs. log(f) [Hz]: for (a) compositions FVNB0, FVNB5 and FVNB15 at 200 °C, (b) FVNB5 at different temperatures.

In Eq. (8), τ_σ is known as conductivity relaxation time and is used to represent electric field decay in an ionic glass as $E = E_0 \exp(-t/\tau_\sigma)$. It suggests that in the limits $\omega\tau_\sigma \ll 1$ and $\omega\tau_\sigma \gg 1$, M' becomes zero and $1/\varepsilon_s$, respectively and so as M''. But at $\omega\tau_\sigma = 1$, M'' gives rise to a peak which is called a relaxation (resonance) peak.

The variation of real parts of the electric modulus M' and imaginary parts of the electric modulus M'' as a function of frequency for FVNB0, FVNB5, and FVNB15 at 200 °C are shown in Fig. 14a and Fig. 15a, respectively. The variation of M' and of M'' as a function of frequency for sample FVNB5 at various temperatures are shown in Fig. 14b and Fig. 15b, respectively. The electric modulus M' profile in Fig. 14 shows that the curve almost tends to zero in the low frequency range and it is due to the suppression of electrode polarization. At higher frequencies, in turn, it reaches M'_∞ because of relaxation process over a range of frequencies. Also the variation of M' shows that M' becomes almost constant at higher frequencies. The zero value of M' at low frequencies marks the non-existence of restoring force for the flow of charge carriers. The shape of M'' curve in Fig. 15 is broader than ideal Debye curves and asymmetric in nature. The maximum in the imaginary part of the electric modulus M'' shifts to higher frequencies with

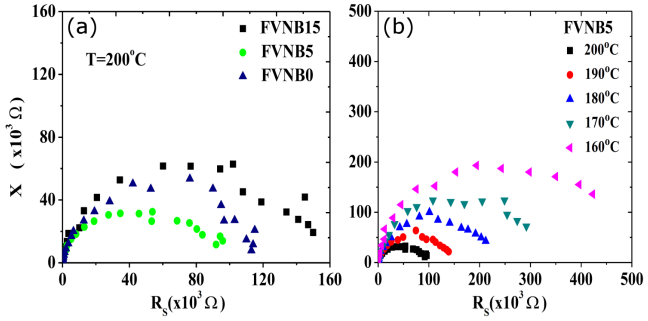

Fig. 16. Nyquist diagrams vs. R_s for (a) compositions FVNB0, FVNB5 and FVNB15 at 200 °C, (b) FVNB5 at different temperatures.

increase in temperature, which shows that the number of charge carriers increases by thermal activation achieved through phonon absorption. The peak frequency corresponding to $M''_{\max}$ corresponds to relaxation time τ_σ, which satisfies the Arrhenius law. The smaller value of M'' at low frequencies indicates negligible contribution of electrode polarization to the electric modulus. Two apparent relaxation regions appear above and below $M''_{\max}$, the low frequency region ($f < f_m$) determines the range in which charge carriers are mobile over long range distance, whereas in high frequency region ($f > f_m$), the charge carriers are confined to potential well, being mobile on short distances and associated with the relaxation polarization process [27, 42–44]. An effective interaction between charge carriers establish correlation between ions and governs non-bridging oxygen sites in the glass. This is possibly the prime cause of appearance of the non-Debye conductivity relaxation in glass compositions under study.

4.4. Impedance spectroscopy

The Nyquist plots [25] for FVNB0, FVNB5, and FVNB15 at 200 °C are shown in Fig. 16a. The impedance data analysis shows that a single semicircle arc is present in all the prepared compositions and there is no residual semicircle at lower frequency, which attributes to the single conduction mechanism [43, 44]. The centre of each semicircle is observed to be depressed below R_s axis which indicates that the associated relaxation of ions is non-Debye in nature [19, 37]. From analysis, the semicircle arcs passing through the origin of impedance plots and the intercept at lower frequency on the R_s axis give bulk resistance R_b. The value of R_b is highest for FVNB0 (i.e., 0 mol% of Fe_2O_3). With increase in concentration of Fe_2O_3, the value of R_b first decreases and then increases, i.e., a non-linear variation of R_b is observed, which indicates the mixed effect of iron and vanadium in the glassy matrix. The Nyquist plots for FVNB5 at different temperatures are shown in Fig. 16b. A single semi-circle in these plots indicates a single conduction mechanism in the FVNB5 sample. The depression of the semi-circle in these plots on the real axis shows that the relaxation

mechanism is non-Debye in nature. The intercepts on the real axis corresponding to zero value of the imaginary axis in the Nyquist plot gives us the bulk resistance of the sample excluding the polarization effects [27, 44]. The values of bulk resistance were found to decrease with increase in temperature and hence DC conductivity of the sample increases with increase in temperature depicting the semi-conducting nature of the sample under study.

5. Conclusion

The structural, physical, and electrical properties of $x\mathrm{Fe_2O_3} + (30 - x)\mathrm{V_2O_5} + 30\mathrm{Na_2O} + 40\mathrm{B_2O_3}$ (abbreviated as FVNBx), where $x = 0, 2, 3, 5, 7, 10$, and 15, have been studied by XRD, density measurement, FTIR, dielectric, and AC and DC electrical conductivity measurements. Density D of the glass samples increases and molar volume V_m decreases with the replacement of $\mathrm{V_2O_5}$ by $\mathrm{Fe_2O_3}$ content by mole fraction x. This is attributed to the decrease in NBOs due to the conversion of trigonal $\mathrm{BO_{3-}}$ structural units into $\mathrm{BO_{4-}}$ tetrahedral and higher oxygen coordination units (pyro- and orthoborates/vanadates) indicating the increase in compactness of the glass network structure. The marginal decrease in the theoretical optical basicity Λ_{th} is indicative of the decrease in ability of oxygen to donate electron. No boroxol rings formation were observed in the structure of these glasses. This suggests that glasses under study consist of randomly connected M–B–O groups, where M=O/Fe/V/Na.

The FTIR spectra and thermal analysis of the present glass systems indicate that $\mathrm{Fe_2O_3}$ acts both, as a glass former and as a glass modifier. It is observed that the thermal cum chemical stability of the glasses is increased by higher concentrations of iron. Therefore, the higher iron contents makes the glass network more and more stable, by participating into the glass network formation.

The temperature dependence of DC conductivity confirms the semiconducting nature of the electrical conduction. Typically, the SRPH mechanism is attributed to the electrical conduction. Iron free glass shows a higher conductivity as compared to iron containing $x > 0$ glasses under study. The increase of NBOs resulted in hindrance to the SRPH. Mixed effect of iron and vanadium ions was identified through the variation of AC and DC conductivity. It was confirmed that the glasses behave as non-polar dielectrics. Average σ_{ac} (at 1 kHz and 200 °C) is ≈ 0.07 μS/m, which is comparable to the average DC conductivity at 80 °C ($\sigma_{av} \approx 0.08$ μS/m) for iron containing glasses (i.e., $x > 0$). The average activation energy W_{av} is ≈ 0.70 eV for iron containing glasses (i.e., $x > 0$). The DC conductivity at 180 °C increases consistently with the increase in x and tends to overshoot the conductivity of FVNB0 glass.

Acknowledgments

Authors are thankful to Central Instrumentation Lab (CIL), DCRUST, Murthal for providing FTIR, thermal, and electrical measurement facilities. Arti Yadav is thankful to UGC for providing financial support under Dr. D.S. Kothari Post Doctoral Fellowship Scheme.

References

[1] D.L. Griscom, *Borate Glasses*, New York 1978.

[2] H. Scholze, *Glass*, Springer-Verlag, New York 1991.

[3] N.P. Bansal, R.H. Doremus, *Handbook of Glass Properties*, Academic Press (Indian Reprint) (2006).

[4] M. Regan, C.F. Drake, *Mater. Res. Bull.* **6**, 487 (1971).

[5] M. Nagaswa, H. Watanabe, *UK Patent No. 1358930*, 1971.

[6] P. Jozwiak, J.E. Garbarczyk, M. Wasiucionek, I. Gorzkowska, F. Gendron, A. Mauger, C.M. Julien, *Solid State Ion.* **179**, 46 (2008).

[7] J.E. Garbarczyk, P. Machowski, M. Wasiucionek, W. Jakubowski, *Solid State Ion.* **157**, 269 (2003).

[8] E.I. Kamitsos, M.A. Karakassides, G.D. Chryssikos, *J. Phys. Chem.* **90**, 4528 (1986).

[9] E.I. Kamitsos, G.D. Chryssikos, A.P. Patsis, M.A. Karakassides, *J. Non-Cryst. Solids* **131-133**, 1092 (1991).

[10] L. Bih, M. El Omari, J.M. Réau, M. Haddad, D. Boudlich, A. Yacoubi, A. Nadiri, *Solid State Ion.* **132**, 71 (2000).

[11] A. Langar, N. Sdiri, H. Elhouichet, M. Ferid, *J. Alloys Comp.* **590**, 380 (2014).

[12] A. Mekki, G.D. Khattak, D. Holland, M. Chinkhota, L.E. Wenger, *J. Non-Cryst. Solids* **318**, 193 (2003).

[13] A.A. Bhagat, *J. Non-Cryst. Solids* **226**, 155 (1998).

[14] G. Dalba, P. Fornasini, F. Rocca, F. Monti, *Phys. Chem. Glass.* **41**, 290 (2000).

[15] R.A. Montani, M. Levy, J.L. Souquet, *J. Non-Cryst. Solids* **149**, 249 (1992).

[16] S. Khasa, M.S. Dahiya, A. Agarwal, P. Chand, *J. Mol. Struct.* **1079**, 15 (2015).

[17] S. Khasa, M.S. Dahiya, A. Agarwal, *J. Mol. Struct.* **1086**, 172 (2015).

[18] A. Yadav, S. Khasa, A.M.S. Dahiya, A. Agarwal, P. Chand, *Spectrochim. Acta A* **157**, 129 (2016).

[19] I. Kashif, S.A. Rahman, A.A. Soliman, E.M. Ibrahim, E.K.A. Khalek, A.G. Mostafa, A.M. Sanad, *Physica B* **404**, 3842 (2009).

[20] S. Saetova, A.A. Raskovalov, B.D. Antonov, T.V. Yaroslavtseva, O.G. Reznitskikh, E.V. Zabolotskaya, N.I. Kadyrova, A.A. Telyatnikova, *Ionics* **24**, 1929 (2018).

[21] J.A. Duffy, E.I. Kamitsos, G.D. Chryssikos, A.P. Patsis, *J. Phys. Chem. Solids* **34**, 153 (1993).

[22] V. Dimitrov, T. Komatsu, *J. Ceram. Soc. Jpn.* **107**, 1012 (1999).

[23] J.A. Duffy, M.D. Ingram, *J. Non-Cryst. Solids* **21**, 373 (1976).

[24] J. Duffy, M. Ingram, *J. Am. Chem. Soc.* **93**, 6448 (1971).

[25] R. Iordanova, Y. Dimitriev, V. Dimitrov, D. Klissurski, *J. Non-Cryst. Solids* **167**, 74 (1994).

[26] S. Muthupari, S. Prabhakar, K.J. Rao, *J. Phys. Chem.* **98**, 2646 (1994).

[27] B. Tareev, *Physics of Dielectric Materials*, MIR Publ., Moscow 1979.

[28] N.F. Mott, *J. Non-Cryst. Solids* **1**, 1 (1968).

[29] M.S. Dahiya, S. Khasa, A. Agarwal, *J. Therm. Anal. Calorim.* **123**, 457 (2016).

[30] J.A. Kerr, *Chem. Rev.* **66**, 465 (1966).

[31] A. Yadav, S. Khasa, M.S. Dahiya, S. Dalal, A. Hooda, A. Agarwal, *Phys. Chem. Glass.* **57**, 146 (2016).

[32] B. de B. Darwent, *National Standard Reference Data Series: Bond Dissociation Energies in Simple Molecules*, National Bureau of Standards No. 31, Washington 1970.

[33] I.G. Austin, N.F. Mott, *Adv. Phys.* **18**, 41 (1969).

[34] T.K. Pietrzak, P.P. Michalski, P.E. Kruk, W. Ślubowska, K. Szlachta, P. Duda, J.L. Nowiński, M. Wasiucionek, J.E. Garbarczyk, *Solid State Ion.* **302**, 45 (2017).

[35] L. Murawski, R.J. Barczyński, D. Samatowicz, *Solid State Ion.* **157**, 293 (2003).

[36] V. Naresh, S. Buddhudu, *Ferroelectrics* **437**, 110 (2012).

[37] A. Langar, N. Sdiri, H. Elhouichet, M. Ferid, *J. Alloys Comp.* **590**, 380 (2014).

[38] N. Singh, A. Agarwal, S. Sanghi, *J. Alloys Comp.* **509**, 7543 (2011).

[39] M.P. Kumar, T. Sankarappa, B.V. Kumar, N. Nagaraja, *Solid State Sci.* **11**, 214 (2009).

[40] P.B. Macedo, T. Moynihan, R. Bose, .

[41] A.A. Bhagat, *J. Non-Cryst. Solids* **226**, 155 (1998).

[42] D.D. Ramteke, R.S. Gedam, *Spectrochim. Acta A* **133**, 19 (2014).

[43] A. Hooda, S. Sanghi, A. Agarwal, R. Singh, N. Ahlawat, *J. Appl. Phys.* **112**, 014110 (2012).

[44] S. Sanghi, S. Duhan, A. Agarwal, P. Aghamkar, *Physica B* **405**, 3846 (2010).